Published in final edited form as:
Magn Reson Med. 2013 December ; 70(6): . doi:10.1002/mrm.24622.

Induced Clustered Nanoconfinement of Superparamagnetic Iron Oxide in Biodegradable Nanoparticles Enhances Transverse Relaxivity for Targeted Theranostics

Ragy R. T. Ragheb[1], **Dongin Kim**[1], **Arunima Bandyopadhyay**[1], **Halima Chahboune**[1], **Beyza Bulutoglu**[1], **Harib Ezaldein**[1], **Jason M. Criscione**[1], and **Tarek M. Fahmy**[1,2,*]

[1]Department of Biomedical Engineering, Yale University, New Haven, Connecticut, USA.

[2]Department of Chemical Engineering, Yale University, New Haven, Connecticut, USA.

Abstract

Purpose—Combined therapeutic and diagnostic agents, “theranostics” are emerging valuable tools for noninvasive imaging and drug delivery. Here, we report on a solid biodegradable multifunctional nanoparticle that combines both features.

Methods—Poly(lactide-*co*-glycolide) nanoparticles were engineered to confine superparamagnetic iron oxide contrast for magnetic resonance imaging while enabling controlled drug delivery and targeting to specific cells. To achieve this dual modality, fatty acids were used as anchors for surface ligands and for encapsulated iron oxide in the polymer matrix.

Results—We demonstrate that fatty acid modified iron oxide prolonged retention of the contrast agent in the polymer matrix during degradative release of drug. Antibody-fatty acid surface modification facilitated cellular targeting and subsequent internalization in cells while inducing clustering of encapsulated fatty-acid modified superparamagnetic iron oxide during particle formulation. This induced clustered confinement led to an aggregation within the nanoparticle and, hence, higher transverse relaxivity, r_2, (294 mM^{-1} s^{-1}) compared with nanoparticles without fatty-acid ligands (160 mM^{-1} s^{-1}) and higher than commercially available superparamagnetic iron oxide nanoparticles (89 mM^{-1} s^{-1}).

Conclusion—Clustering of superparamagnetic iron oxide in poly(lactide-*co*-glycolide) did not affect the controlled release of encapsulated drugs such as methotrexate or clodronate and their subsequent pharmacological activity, thus highlighting the full theranostic capability of our system.

Keywords

PLGA; iron oxide; clustered; targeted; methotrexate; clodronate

Theranostic constructs combine both therapeutic and diagnostic properties in a single platform (1,2). As such, these systems have recently gained significant attention because of their promise in visualizing therapeutic intervention. Recent progress in both the nanotechnology fabrication front and diagnostic modalities are advancing the design and application of these tools for different disease states (3–7). The attractive aspects of the

*Correspondence to: Tarek M. Fahmy, Ph.D., Department of Biomedical Engineering, Yale University, 55 Prospect Street, 401 Malone Engineering Center, New Haven, CT 06511. tarek.fahmy@yale.edu.

Additional Supporting Information may be found in the online version of this article.

approach stems from the idea that such systems can simultaneously function to improve drug therapy by localizing drug delivery (6,8–11), guide the delivery process by visualizing the biodistribution of nanoparticle-based therapies and hence facilitate "positioning the dose" for early-stage particulate-based drug development process (6,8–11), or improve upon conventional therapies such as radiation or hyperthermia (12–14). Toward that goal of combining multiple functionalities into a single platform, one of the encumbering issues remains optimization of the therapeutic and imaging agent concentrations in the theranostic platform for realization of effective localized drug delivery and noninvasive imaging. Progress in this area, especially with safe biodegradable materials will yield an optimal platform that function effectively for both treatment and monitoring of targeted drug delivery.

Of the different imaging systems available to researchers and clinicians, magnetic resonance (MR) imaging is attractive for noninvasive imaging. Not only because of its ability to image deep into tissue with sufficient sensitivity, and spatiotemporal resolution through the use of appropriate contrast agents, but also because of its safety, wide availability of magnetic resonance imaging (MRI) scanners, and hence, clinical relevance. In MR, the signal strength is directly related to the relaxation rates of protons in the local environment, (r1, the longitudinal relaxation rate, and r_2, the transverse relaxation rate). Because of this correlation, agents that enhance the rate of either relaxation are important as MR contrast agents. While commercially available dextran-coated superparamagnetic iron oxides (SPIOs) (e.g., Molday Ion) are excellent r_2 (or T_2-inverse relaxation rate) contrast agents, their theranostic utility is limited (Table 1) (15). For example, dextran-coated SPIO are limited in their drug loading capacity and the weak associations of these coatings can often lead to aggregation and precipitation under physiological conditions (16). For these reasons, alternative iron-oxide-polymer hybrid systems (3,4,17–20) have been sought. Of those, polyester-based systems, such as poly(lactide), poly(glycolide), or their copolymer (poly(lactide-*co*-glycolide) (PLGA)), coated iron oxides have gained attention because of their established physiological biocompatibility, tunable biodegradation, and well-understood formulation conditions for encapsulation and release of a wide range of therapeutics (21–23). These iron-oxide-polymer hybrid systems are nontoxic and have demonstrated utility for in vivo cell tracking and therapeutic delivery such as simultaneous priming of antigen and imaging of cell trafficking (22).

In this work, we developed a multifunctional theranostic platform that facilitates targeting through a new method for surface modification of biodegradable polyester systems (24), controlled release of therapeutics, and maintenance of MR imaging capability during controlled release. One of the main motivations behind the design of the platform was to demonstrate the ability to not only incorporate multiple functions but to introduce a methodology for maintaining imaging capabilities during controlled release. We demonstrate the versatile use of fatty acids as hydrophobic anchors that strongly associate with the PLGA matrix (24,25), affording presentation of targeting ligand conjugates on the PLGA nanoparticle surface to increase cellular targeting and internalization into cells. Furthermore, we show that fatty acids not only allow co-encapsulation and prolonged retention as hydrophobic stabilizers for SPIO, but afford varying degrees of SPIO aggregation resulting in an enhanced and controllable system for MR imaging. This system, thus, preserves biocompatibility and maintains imaging characteristics without hindering the controlled release of small-molecule therapeutics.

METHODS

Materials

PLGA 50:50 with an inherent viscosity of 0.59 dL/g (Lactel Polymers, Inc., Pelham, AL) was used as received. Polyvinyl alcohol (M_w average 30–70 kD) was obtained from Sigma-Aldrich. Chloroform was of chromatography grade and supplied by Fisher Scientific. Iron acetylacetonate ($Fe(acac)_3$, Aldrich, 99+%), oleic acid (Sigma-Aldrich, 99%), oleylamine (Aldrich), 1,2-hexadecanediol (Aldrich, 90%), and benzyl ether (Aldrich, 99%) were used as received. Coumarin 6 (C-6) (laser grade) was supplied by Acros Organics. Methotrexate (MTX) and dichloromethylenediphosphonic acid disodium salt (Clodronate disodium) (Clod) were obtained from Sigma-Aldrich.

Cells

Macrophages were generated from bone marrow cells collected from the femurs and tibias of mice. Cells were RBC lysed with ammonium chloride (Sigma), and cultured for 7 days in complete RPMI medium (RPMI supplemented with 10% fetal bovine serum (FBS), 1% L-glutamine, 1% N-2-hydroxyethylpiperazine-N'-2-ethanesulfonic acid (HEPES) buffer, nonessential amino acids, 0.1% 2-ME, 50 μg/mL streptomycin, 50 IU/mL penicillin) and 10 ng/mL recombinant m-colony stimulating factor (CSF) and 1 ng/mL recombinant murine GM-CSF. After every 2–3 days, non-adherent cells were discarded and fresh media containing growth factors was added to the culture. Adherent cells were dislodged using cell dissociation buffer (Invitrogen). Flow cytometry confirmed that >99% of the cells were $CD11b^{hi}$. The murine macrophage cell line (Raw 264.7) and B16 tumor cells were purchased from ATCC and cultured in complete growth media (Dulbecco's modified eagle medium (DMEM)+ 10% FBS+2% penicillin/streptomycin). After reaching confluence, the cells were detached using trypsin-ethylenediaminetetraacetic acid (EDTA).

Synthesis of SPIO

$Fe(acac)_3$ (0.396 g, 1.56 mmol), oleic acid (1.47 mL, 4.64 mmol), oleylamine (1.02 mL, 3.09 mmol), 1,2-hexadecanediol (2.005 g, 7.76 mmol), and benzyl ether (10 mL) were added to a single-neck round-bottom flask equipped with a magnetic stir bar and a condenser and deoxygenated for an hour. The reaction was gradually heated at 3° C/min to 200° C and held at that temperature for 3 h and then allowed to cool room temperature. A final black solution was observed. The reaction mixture was precipitated in ethanol and centrifuged twice. Ethanol was decanted and the product was dried via nitrogen purge leaving a black powder.

Preparation of SPIO-Loaded Nanoparticles

PLGA nanoparticles encapsulating hydrophobic SPIO were prepared and surface-functionalized as described previously (24,25). Briefly, PLGA (107 mg) and hydrophobic SPIO (26 mg) were dissolved in chloroform (2 mL) and then added drop-wise to a vortexing solution of 5% polyvinyl alcohol (4 mL), and the resulting mixture was sonicated three times for 10 s at an amplitude of 38% (TEKMAR VCW 400 W). The mixture was then added drop-wise to 100 mL of 0.2% polyvinyl alcohol and left stirring for 3 h to evaporate the solvent. Particles were collected by centrifugation at 12,000 RPM for 10 min at 4° C and then washed three times with deionized water. The particles were lyophilized and stored at −20° C until use. Particles functionalized on the surface with avidin were prepared in identical fashion with avidin-palmitate (25) incorporated into the 5% polyvinyl alcohol solution. Nanoparticles that encapsulating C-6 and functionalized with avidin were manufactured using a modified double emulsion variation of the water-oil-water technique. Nanoparticles encapsulating magnetite and MTX (dissolved in DMSO) were prepared using

a single emulsion. Nanoparticles encapsulating magnetite and Clod were manufactured in a similar fashion using a double emulsion, water-oil-water technique.

Thermogravimetric Analysis

Thermogravimetric analysis (TGA) was performed on a TGA Q1000 from TA Instruments, Inc. TGA samples (3–4 mg) were ramped from 50 to 800° C at 10° C/min in a N_2 environment.

Superconducting Quantum Interference Device

Magnetization curves were taken using a Quantum Design Magnetic Properties Measurement System, which uses superconducting quantum interference device (SQUID) technology. The magnetization was measured while changing the external magnetic field between ± 3 T. The lack of noticeable hysteresis in the M(H) loop, taken at T=298 K, reveals the superparamagnetic behavior of the iron oxide nanoparticles (2–4 mg).

Transmission Electron Microscopy

Transmission electron microscopy (TEM) examination of the SPIO and the SPIO-loaded PLGA nanoparticles were evaluated on a PHILIPS Tecnai T12 HR-TEM, operating at 120 kV and digital electron micrographs were acquired with a high-resolution 4 k × 4 k GATAN Ultrascan charge-coupled device camera. A drop of well-dispersed nanoparticle suspension was placed on an electron microscopy services carbon film 400 mesh copper grid and then dried at ambient conditions before placement in the sample holder of the microscope. Size distribution and average particulate diameter of iron oxides were determined by analyzing 150 particulates per image using the freeware program NIH ImageJ.

Scanning Electron Microscopy

Scanning electron microscopy (XL-30 ESEM FEG, FEI Company) was used to visualize lyophilized nanoparticles. Blank PLGA, SPIO-loaded PLGA, and SPIO-loaded PLGA with avidin surface functionality were visualized with scanning electron microscopy. The particles were fixed on an aluminum stub using 2-sided carbon tape and then coated with carbon in an argon atmosphere using a sputter coater (Cressington C208 with a rotational table and thickness monitor). The samples were imaged with a scanning electron microscope using a LaB electron gun with an accelerating voltage of 5–10 kV.

Inductively Couple Plasma Mass Spectrometer

The iron content of the SPIO-loaded PLGA nanoparticles were determined by using an inductively couple plasma mass spectrometer (ELEMENT XR, Thermo Scientific, USA). 56Fe was measured using medium resolution (4000) and high resolution (10,000) mass/mass difference. Under these conditions, $^{40}Ar^{16}O$, which only needs a resolution of ~2500 (mass/mass difference), was readily distinguished from 56Fe. Concentrated nitric acid and hydrogen peroxide were added to completely digest the samples to release iron for analysis.

Nanoparticle Size Analysis

NanoSight with an LM10 Topdown Microscope, NTA 2.0 Software, and Marlin Camera was used to visualize and determine the size distribution and concentration of nanoparticles. The nanoparticles were dispersed in phosphate buffered saline (PBS) at dilute concentrations prior to analysis (20 μg/mL). NanoSight's "Nanoparticle Tracking Analysis" detects and visualizes populations of nanoparticles in liquids and measures the size of each particle from direct observations of diffusion (26).

Coupling of Ligands to the Nanoparticle Surface

The amount of avidin per mg of the nanoparticles was quantified using the Micro BCA Protein assay. Biotinylated anti-mouse F4/80 mAb (eBioscience) was added at various concentrations (0–20 μg/mL) to a 5 mg/mL solution of PLGA particles in PBS and rotated for 20–30 min at room temperature. The nanoparticles were then centrifuged at 10,000 rpm for 10 min and the supernatant was retained to measure the amount of unbound Ab remaining using the Micro BCA Protein Assay Kit. Biotinylated RGD peptide was conjugated to avidin on the surface of the particles for targeting to B16 tumor cells.

Assessment of Nanoparticle Internalization by Flow Cytometry

Macrophages were plated at 10^6 cells/mL in RPMI media+10% FBS supplemented with L-glutamine, MEM nonessential amino acids, HEPES buffer, gentamicin, and β-mercaptoethanol in a 24-well plate for 2 h to allow adherence. These cells were then incubated with 100 μg/ mL of C-6-loaded nanoparticles for 2 h. These nanoparticles were either nontargeted or targeted on the surface with anti F4/80, a macrophage specific antibody. After 2 h, the cells were washed twice with PBS+1% FBS. The cells were labeled with APC-conjugated $CD11_b$ mAb (eBioscience) for 30 min at 4° C. Cells were then washed with PBS+1% FBS and then fixed with 2% paraformaldehyde. These cells were then analyzed by flow cytometry analysis using a FACS Calibur system (BD).

Assessment of Nanoparticle Internalization by Confocal Microscopy

Macrophages were plated on glass cover slips (2×10^5 cells per cover slip) for 2 h at 37° C for adherence. Cells were then incubated with 100 μg/mL of nanoparticles for 2 h at 37° C. Targeted and nontargeted C-6 loaded nanoparticles were used for this assay. After 2 h, media was removed and cells were washed with PBS+1% FBS and then fixed in 2% paraformaldehyde. 0.1% Triton-X 100 in PBS was used to permeabilize the cells and then stained with a 1:200 dilution of Alexa 548-phalloidin and 1:500 dilution ToPro-3 (Molecular Probes) to delineate the cytoskeleton and nucleus, respectively. Cells were visualized under Zeiss confocal microscope (LSM 510) using wavelengths 488, 568, and 633 nm.

DiI-Ac-LDL Uptake Assay

Acetylated low-density lipoprotein labeled with 1,1-dioctadecyl- 3,3,3′,3′-tetramethylindocarbocyanine perchlorate (DiI-Ac-LDL) was purchased from Biomedical Technologies (Stoughton, MA). bone marrow-derived macrophages (BMDMs) at a concentration of 1×10^6 cells were plated in each well in a 24-well plate and allowed to adhere for a few hours. Both targeted and nontargeted nanoparticles at varying concentrations from 100 μg/mL to 800 μg/mL were added to each well for 2 h. After 2 h, cells were washed 3× with sterile PBS. DiI-Ac-LDL was added at a concentration of 10 μg/ mL in complete growth media to each well for 4 h at 37° C. This concentration of DiI-Ac-LDL has been shown to have no effect on cell viability. After 4 h, the media containing the DiI-Ac-LDL was removed from culture and cells were washed 3× with PBS. The cells were then fixed in 3% formaldehyde, dislodged using cell dissociation buffer (Invitrogen), and analyzed for fluorescence at 520/564 nm using flow cytometry.

Cell Viability Assay

Cell titer blue viability assay was purchased from Promega, Madison, WI. Cells were incubated with SPIO-PLGA nanoparticles loaded with either MTX or Clod and compared with soluble drug, media, cells alone, and azide. Cells were plated at a density of 5×10^4 cells per well in black opaque walled 96-well plates (Corning Costar, NY). Nanoparticles were incubated in triplicate with cells at different concentrations (250–8000 μg/mL) for 24 h followed by the addition of 40 μL of Cell titer blue to each well and incubated at 37° C for 3

h. Free MTX and Clod concentrations were 3.125–100 μM and 3.125–100 mM, respectively. After 3 h, the number of viable cells was measured using fluorescence at 560/590 nm.

MR Relaxometry

T_2-weighted MR images of serially diluted Molday Ion and SPIO-PLGA nanoparticles in triplicate in PBS were acquired on a Varian 9.4 T horizontal bore magnet using a bird cage coil to determine the r_2 value of the developed nanoparticles, T_2-relaxation measurements were obtained using a multi-slice multi-echo sequence with the number of echoes=10, echo time/pulse repetition time=10/4000 ms, a field of view of 28 mm, a matrix size of 128 × 128, and a slice thickness was 1 mm. MR data was analyzed with homemade software using Matlab 5.6.1 (Math-Works). Pixel-by-Pixel T_2-maps were calculated by performing fits of multiple images to a monoexponential decay. T_2-relaxation times were derived by region of interest measurements of the samples on the T_2-maps, and subsequent conversion to R_2 relaxation rates ($R_2=1/T_2$). The transverse relaxivity was calculated from the slope of the graph of R_2 ($1/T_2$) versus iron concentration.

MRI Phantom Imaging of Labeled Macrophages

RAW 264.7 (ATCC) cells were cultured in complete media (DMEM+10% FBS+2% Penicillin/Streptomycin). Cells at a concentration of 10×10^6 cells were plated into each T75 flask and were allowed to adhere overnight resulting in 80% confluence the next day. The cells in each T75 flask were incubated with SPIO-loaded PLGA nanoparticles with F4/80 or nontargeted nanoparticles at a concentration of 1 mg/mL in serum free media (DMEM with Penicillin/Streptomycin, but no FBS) in a total volume of 10 mL of media for 2 h. The flasks were agitated every 30 min to prevent the nanoparticles from settling. After the 2 h of incubation, cells were dislodged using a cell scraper, collected, washed 4× with PBS, and fixed with 3% formaldehyde for 20 min at room temperature. The total cell number in each vial prepared for MR imaging was 1×10^7. The ratios of labeled cells to unlabeled cells were 4:0, 3:1, 2:2, 1:3, and 0:4. The cells were finally suspended in 400 μL of PBS with 400 μL of a 10% gelatin solution to make a homogeneous suspension.

MR images were acquired on a Varian 9.4 T horizontal bore magnet as previously described. To determine the r_2 of the developed nanoparticles, T_2 measurements were performed on a serial dilution of the nanoparticles in gelatin. Phantoms containing different concentrations of labeled macrophages with 1.0 mg/mL SPIO-loaded PLGA nanoparticles targeted to F4/80 or nontargeted were imaged.

Prussian Blue Staining

Prussian blue staining was performed to detect the presence of internalized iron. Murine macrophage cells (RAW 264.7) and B16 tumor cells were cultured in DMEM media as previously mentioned. After reaching confluence, the cells were detached using trypsin-EDTA, and 2×10^5 cells were seeded into a glass cover slips for overnight for adherence. Macrophage cells were washed with PBS three times and then incubated with varied concentration of either anti-F4/80 coated nanoparticles or without anti-F4/80 nanoparticles from 100 to 400 μg/ mL for 2 h either at 37° C or 4° C. Tumor cells were washed with PBS three times and then incubated with varied concentrations of either RGD-coated nanoparticles or untargeted particles from 100 to 400 μg/mL for 2 h either at 37° C or 4° C. After treatment, the cells were washed briefly twice in PBS and fixed with 10% neutral buffered formalin (Sigma-Aldrich, St. Louis, MO) for 10 min. After washing in PBS, samples were stained with a filtrated 2% potassium ferrocyanide II/1 M hydrochloric acid mixture (ratio 1:1) for 10 min at 37° C causing a deep blue complex. Then, cells were washed with PBS and subsequently counterstained with a 0.1% (w/v) solution of Nuclear

Fast Red (Chroma, Stuttgart, Germany) in distilled water with 5% aluminum sulfate, for 1 min. After washing with distilled water, the images of cell were obtained through Nikon (TE2000-U) electron microscope.

In Vivo Biodistribution

Mice were housed in autoclaved micro-isolator cages that were placed in a positive pressure containment rack and maintained according to an approved protocol from the Yale University Institutional Animal Care and Use Committee. The mice were randomly assigned to experimental and control groups of four animals each. B16 tumor cells were cultured in DMEM media with 10% FBS and 2% antibody. After reaching confluence, the cells were detached using trypsin-EDTA. The melanoma xenografts were initiated by subcutaneously implanting the detached B16F10 cells (5×10^6 cells) in the right rear flank of the mice. After 10 days, each mouse was treated with a different nanoparticle formulation. Mice were injected with 64 μg SPIO/C-6-loaded PLGA nanoparticles decorated with avidin/biotinylated PEG (2000) or 4 μg Molday Ion via the tail vein. After injection, the mice were euthanized at each time point (1, 6, 15 h postinjection) for biodistribution. Each organ including heart, lung, liver, kidney, spleen with blood, and tumor was excised. The C-6 intensity of all organs and tumor were directly imaged using a molecular imaging instrument (Carestream In Vivo MS FX Pro®) The C-6 intensity of all the blood samples were imaged after freeze-drying and dissolution into a co-solvent of DMSO with 10% 1 N NaOH. Standard curves were generated for C6. Fluorescence of the supernatant was determined by the excitation/emission of 460/540 nm to calculate C-6 concentration.

RESULTS

Synthesis of SPIO

SPIO nanoparticles are commonly produced via co-precipitation of ferrous (Fe_{2+}) and ferric (Fe_{3+}) ions by a base, usually NaOH, or $NH_3{\cdot}H_2O$, in an aqueous solution (27,28). One of the disadvantages of this procedure is that the pH value of the reaction must be adjusted both in the synthesis and the purification, and thus, leading to limited yields of small (<20 nm) monodisperse nanoparticles. In this study, $Fe(acac)_3$ was reacted with oleic acid and oleylamine in benzyl ether affording a versatile seed-growth reaction system for nonaqueous preparation of magnetite nanoparticles (Fig. 1a). The reaction of $Fe(acac)_3$ with surfactants at high temperature lead to the controlled growth of monodisperse Fe_3O_4 nanoparticles that were easily separated from byproducts and the ether solvent resulting in the formation of a magnetic black powder (29). TEM showed discreet magnetite nanoparticles with relatively uniform size and shape (Fig. 1b) ranging from 4 to 10 nm with the average of 7 nm (Fig. 1c). The magnetic properties of the magnetite nanoparticles were measured with super quantum interference device (SQUID) technology and indicate superparamagnetic behavior at room temperature as evidenced by an absence of hysteresis (Fig. 1d).

Preparation of SPIO-Loaded PLGA Nanoparticles Functionalized With an Adaptor Molecule (Avidin)

SPIO-loaded PLGA nanoparticles have been previously demonstrated (7,30,31). In these studies, SPIO-loaded PLGA nanoparticles were prepared using a water-oil-water double emulsion and incorporating commercial aqueous magnetite (e.g., Resovist). Stabilizing magnetite with oleic acid and oleylamine offers increased surface hydrophobicity resulting in effective incorporation of magnetite into the oil phase of the PLGA nanoparticle preparation (Fig. 2a). This further prevents undesired release of as noted through inductively couple plasma mass spectrometer (Fig. 2b).

To demonstrate that targeting may enhance cell-specific attachment and, therefore, potentially increase internalization in phagocytic cells, avidin-based targeting ligands were presented on the surface of the nanoparticles via an avidin-palmitate conjugate (24,25). Here, the palmitate aliphatic chain partitions into the PLGA matrix, while the avidin segregates to the nanoparticle surface.

Scanning electron microscopy showed relative uniformity and discreteness for blank nanoparticles (Fig. 2c), SPIO-loaded PLGA (Fig. 2d), and SPIO-loaded PLGA with avidin surface functionality (Fig. 2e). The mean hydrodynamic diameters of the nanoparticles were determined by NanoSight® (Table 2). Weight percent of magnetite was determined by TGA by specifically noting the char yields. PLGA nanoparticles encapsulating magnetite with and without avidin correlated closely with the respective original magnetite charge (Table 2). This method proved to be an easy and effective way to introduce a heavy hydrophobic payload in the core of the particle while incorporating stable functionality to the surface.

Nanoparticle Relaxivity Measurements

To demonstrate that incorporation of hydrophobic magnetite into PLGA nanoparticles did not deter the system's imaging capabilities, T_2-weighted images of samples in PBS with decreasing particle concentrations were measured at room temperature in triplicate. The r_2 was determined by the slope of a linear fit of $1/T_2$ versus iron concentration (Fig. 3a). The r_2 value of the avidin-functionalized SPIO-PLGA nanoparticles (294 mM^{-1} s^{-1}) was greater than unmodified SPIO-PLGA nanoparticles (160 mM^{-1} s^{-1}) and both were observed to be higher than that of commercially available iron oxide nanoparticles, Molday Ion (BioPal, USA) (89 mM^{-1} s^{-1}). We noted that increasing concentrations (0, 5, 10, 50 μg/mL) of palmitate-avidin resulted in increased relaxivities. TEM revealed loading of discrete SPIO into PLGA nanoparticles (Fig. 3b). DSPE-PEG was used to further validate the observation that a hydrophobic tail, besides a fatty acid, can be used to induce clustering of the fatty acid modified iron-oxide in PLGA particles during emulsion formation (Fig. 3b). The size difference (hydrodynamic diameter) between the hydrophobic tail and the hydrophilic component of DSPE-PEG (~1 nm DSPE: 4–5 nm PEG) is similar to the size difference of palmitic acid-avidin (~1 nm palmitic acid: 5 nm avidin). Nanoparticles fabricated with and without soluble avidin showed no aggregation proving that the aggregation was not a function of the presence of avidin. TEM of blank PLGA nanoparticles served as a control.

Effect of Macrophage Targeting on Magnitude of Nanoparticle Internalization

Macrophages are capable of phagocytosing particles using various receptors, such as FcR, complement, and scavenger receptors (32). To ascertain conditions needed for optimal loading of BMDMs, nanoparticles were loaded with the fluorescent dye C-6. C-6 was chosen for this study due to its high hydrophobicity and thus negligible release from the nanoparticles (33). Different concentrations of C-6-loaded PLGA nanoparticles with and without macrophage specific targeting ligands were titrated on BMDMs. We targeted F4/80, a macrophage specific receptor, known to mediate internalization. Flow cytometric analysis revealed that nanoparticles targeted with anti-F4/80 (optimized antibody concentration per particle available in Supporting Information Fig. S2) showed enhanced internalization compared with nontargeted nanoparticles at lower concentrations (100–200 μg/ mL) with the largest difference noted at 200 μg/mL (Fig. 4a). Little difference was observed at saturation levels, 400 μg/mL and greater.

Nanoparticle internalization was further assessed by confocal microscopy. Results correlated with the flow cytometry studies demonstrating that nontargeted particle internalization was dose dependent and almost identical to targeted nanoparticles at a saturating concentration of 400 μg/mL (Fig. 4c).

Prussian blue staining for iron in cells was used to validate internalization. SPIO/C-6-PLGA nanoparticles in macrophages revealed a notable increase in internalization of Fe in cells for particles targeted with anti-F4/80 compared with untargeted particles (Fig. 4d).

Assessment of Macrophage Function After Nanoparticle Internalization

To ascertain if nanoparticles compromise inherent cellular functions, such as metabolic activity, BMDMs were exposed to varying concentrations of targeted and nontargeted nanoparticles before being exposed to DiI-Ac-LDL. When macrophages internalize DiI-Ac-LDL, the LDL is degraded by lysosomal enzymes and the fluorophore DiI accumulates in the cell membrane. The uptake of Ac-LDL in the macrophages, therefore, is an indicator of metabolic activity of active cells (Fig. 4b). B3Z T cell hybridoma, which do not internalize the Ac-LDL, were used as a negative control. Mean fluorescence intensity values from flow cytometry indicate that cells treated with different concentrations of nanoparticles maintain normal metabolic functions. Similar findings were observed with the RAW 264.7 cells (data not shown). These results indicate that this system effectively labels macrophages without altering their physiological functions.

MR Imaging of Labeled Macrophages

We characterized the relaxation properties of the labeled cells in vitro. The transverse relaxation time (T_2) was measured for labeled cells suspended in gelatin. For cells labeled with targeted and nontargeted nanoparticles, the T_2 effect was more pronounced with increasing number of labeled cells (Fig. 5a). In addition, the T_2 relaxometry measurement revealed that the large reduction in T_2 was pronounced in cells labeled with F4/80-targeted nanoparticles compared with nontargeted nanoparticles (Fig. 5b). Targeted nanoparticles had lower cell detection limits (3100 cells/mL), calculated from Figure 5a, compared with Molday Ion (7900 cells/mL). Prussian blue staining further validated internalization results obtained by confocal microscopy and flow cytometry.

Quantification of Drug Release and Retention of Iron Oxide

SPIO-loaded PLGA nanoparticles were loaded with either MTX or Clod (Table 3) and controlled release studies were performed to examine the simultaneous release of drug and retention of magnetite. Quantitative release (100%) of encapsulated MTX was observed over 8 days (Fig. 6a) and 35% of encapsulated Clod was released over the same duration (Fig. 6b). This difference is likely due to the inherent differences in chemical properties of the molecules and their associated drug–polymer interactions. In both cases, negligible percentages of encapsulated magnetite were released. Similar release of MTX and Clod was observed with particles loaded with the drug only, thus iron oxide did not affect the release profiles of the drug.

Assessment of Drug-Loaded Nanoparticles on Macrophage Depletion

Macrophages were incubated with nanoparticles containing SPIO and either MTX or Clod for 24 h and compared with incubation with free MTX, Clod, and blank SPIO-loaded nanoparticles. Blank SPIO-PLGA nanoparticles showed no cytotoxicity up to a concentration of 8 mg/ mL. Cytotoxicity of MTX encapsulated in SPIO-loaded PLGA nanoparticles proved more effective in macrophage depletion than free MTX (Fig. 6c). A similar trend was observed for Clod encapsulated in SPIO-loaded PLGA nanoparticles (Fig. 6d).

Attachment of RGD Peptide to Nanoparticles Facilitates Internalization in a B16 Tumor Cell Line

The B16 tumor cell line is not naturally phagocytic like macrophages but overexpresses αvβ3 integrins, which can facilitate internalization of integrin-specific particles. Targeting specificity was thus tested with particles decorated with biotin-RGD (a ligand to the αvβ3 integrin). Prussian blue staining for Fe in this cell line revealed a notable increase Fe internalization of compared with untargeted particles (Fig. 7a).

In Vivo Biodistribution

To assess in vivo biodistribution of nanoparticles containing SPIO compared with free SPIO, particles were pegylated with biotin-PEG (2)000) and administered to tumor bearing animals. Pegylated nanoparticles distributed primarily to the lung and spleen after 1 h and cleared similarly to free iron after 15 h (Fig. 7b,c). Pegylated particles, however, lasted longer in the blood pool compared with free iron oxide (Fig. 6d). Blood pool distribution differences between the nanoparticle and Molday Ion increased from 2-fold at 6 h to 4-fold at 15 h post IV injection (Fig. 7d). A similar trend was noted in the tumor with sustained increase in pegylated nanoparticle retention compared with Molday Ion (Fig. 7e).

DISCUSSION AND CONCLUSIONS

A capability most highly sought after in therapeutics/imaging reagent platforms is a system that facilitates controlled delivery on target and that retains intrinsic imaging property during this delivery process. Achieving this goal with a biodegradable system is complicated by the very fact that the biodegradability that lends itself to controlled and sustained encapsulated agent delivery may compromise the imaging capability, if the imaging agent is co-encapsulated with the drug. For this reason, we sought to engineer a system that avoids this complication. At the same time, having the ability to independently modulate important features of the system, such as the nature of the drug, targeting of the drug dose, and noninvasive imaging of the targeted dose, enables optimization of the many drugs, targets, and hence application to different disease states.

Toward this end, we designed a nanoparticle platform that confines an MRI imaging agent while enabling controlled drug release and effective cellular targeting. The key to achieving these multiple functions is the incorporation of fatty stabilizers, beginning with the MR contrast agent, SPIO. SPIO is synthesized through the controllable nucleation and growth of magnetic nanoparticles in the presence of hydrophobic stabilizers, oleic acid, and oleylamine. This robust and stable fabrication method offers a narrow size distribution, higher yields, and high reproducibility compared with the common co-precipitation method of two iron salts where small changes in conditions can yield alterations in the products (28,29). The narrow size distribution leads to superparamagnetic behavior, thus preventing undesired agglomeration from remnant magnetization and affording effective SPIO nanoparticle suspension in organic solvents. Stabilizing magnetite with fatty acids, oleic acid, and oleylamine offers increased surface hydrophobicity that leads to the second step, enhanced and long-lasting incorporation of magnetite into the oil phase of the PLGA-based nanoparticle preparation. This is crucial in preventing undesired release of Fe, subsequent nonspecific MRI imaging, and toxic side effects. While several papers report SPIO-loaded nanoparticle systems, iron release from these systems is not considered (4,18,19). The two reported studies that show the encapsulation of a commercially available SPIO, Resovist® (30), or SPIO in PLGA (21) show release of Fe orders of magnitude higher than presented in this work. To the best of our knowledge, our work demonstrates the only significant retention and induced clustering of SPIO in such biodegradable systems. The methodology for retention of the SPIO and surface functionality by the incorporation of fatty acids on

both the SPIO and the surface ligand are couple and lead to the clustering and observed increase in relaxivity.

Interestingly, surface fatty acids for avidin surface presentation enable SPIO aggregate formation, leading to increased r_2 and enhanced overall MR sensitivity. Surface presentation of avidin as a ligand facilitates targeting as demonstrated with F4/80, a macrophage-specific receptor. Here, we note that encapsulation of iron oxide in the biodegradable nanoparticles significantly enhanced the r_2 of native commercial iron oxide, 89 mM^{-1} $s^{-1}$for Molday ion compared with 160 mM^{-1} s^{-1} for SPIO-loaded nanoparticles (Table 2). We showed that surface modification with avidin-fatty acid conjugates induced aggregation of SPIO by TEM. Furthermore, as shown in the inset in Figure 3b, biotinylated gold nanoparticles localized in the regions where clustering of SPIO was observed and thus validated the observation that the avidin-fatty acid regions of the particles were the area where clustering tended to occur. This induced aggregation of SPIO increased the r_2 of SPIO in loaded nanoparticles to 294 mM^{-1} s^{-1}, despite the fact that the amount of SPIO was the same in surface modified and unmodified particles (Table 2). SPIO-loaded PLGA nanoparticles were prepared with an equivalent amount of soluble avidin with subsequent TEM showing discreet nonaggregated SPIO within the core. This highlights the direct effect that avidin tethered to the surface through fatty acid conjugation has on SPIO aggregation within the nanoparticle. We further established the effect of fatty acids by demonstrating that nanoparticles prepared with PEGylated lipids also yield SPIO aggregation. The relaxivity of avidin-functionalized nanoparticles are seemingly controlled by incorporating varying amounts of palmitate-avidin conjugates (5, 10, and 50 μg/mg nanoparticle).

These findings are consistent with previous research showing that clustering of iron oxide via polymer matrix composition or coating of the iron oxide with different polymers increases the r_2 with increased cluster size of SPIO (34–36). In this study, clustering of SPIO was induced via fatty acid-mediated interactions of the surface ligand and the fatty acid on the SPIO. Thus, fatty acids are used here for two main functions: (1) facilitate anchoring of the ligand or SPIO to the polymer matrix, and (2) induce SPIO aggregation within the nanoparticle and thereby increase relaxivity.

A significant feature of this system is the ability to release drug therapeutics while maintaining intrinsic imaging capability. We demonstrated the generality of this feature with two model drugs: MTX and Clod with different physiochemical properties and modes of action. MTX, a hydrophobic folate antimetabolite, is a powerful anticancer agent with substantial side effects and has been shown to deplete macrophages (37), whereas Clod, a hydrophilic drug in the bisphosphonate family, inhibits macrophage viability through induction of apoptosis (38), and because of its hydrophilicity has poor cell membrane permeability. Both drugs are important candidates for targeted nanoparticulate formulations given their high dose administration in therapeutic applications. We showed that nanoparticle mediated delivery of both MTX and Clod effectively inactivated and depleted macrophages at lower concentrations than the respective free forms following cellular internalization (Fig. 6c,d).

To demonstrate the generality of the platform for cellular targeting, we examined cell lines that are not naturally phagocytic but can internalize upon specific coupling to cell surface receptors (B16 tumor cell line). This cell line overexpresses αvβ3 integrins, which can be targeted with RGD modified nanoparticles for internalization. We showed specific internalization (Fig. 7a) with RGD coupled nanoparticles loaded with iron oxide compared with unmodified nanoparticles. In vivo biodistribution with pegylated nanoparticles demonstrated enhanced blood pool kinetics and retention in the tumor microenvironment compared with free iron oxide (Fig. 7b–e). These studies were aimed as proof-of concept

regarding the versatility of the system in attachment of different types of ligands and targeting different cell types. The combination of induced SPIO nanoconfinement within a biodegradable drug releasing nanoparticle for controlled drug delivery to specific cellular targets presents a versatile and effective theranostic platform for potential clinical intervention and diagnosis.

Supplementary Material

Refer to Web version on PubMed Central for supplementary material.

Acknowledgments

We are grateful to Dr. Jodie Lutkenhaus, TengHooi Goh, and Dr. Andre Taylor for use of the TGA in their lab; Dr. Zhenting Jiang for assistance with scanning electron microscopy; Drs. Zhan Peng and Zhengrong Wang for inductively couple plasma mass spectrometer analysis; and Dr. Christoph Rahner for assistance with TEM. We also thank Dr. Judy Riffle (Virginia Tech, Macromolecules and Interfaces Institute) and the members of the Fahmy Lab Group (Yale University) for helpful discussions. Ragy R. T. Ragheb, Dongin Kim, and Arunima Bandyopadhyay contributed equally to this work.

REFERENCES

1. Xie J, Jon S. Magnetic nanoparticle-based theranostics. Theranostics. 2012; 2:122–124. [PubMed: 22287992]
2. Kelkar SS, Reineke TM. Theranostics: combining imaging and therapy. Bioconjugate Chem. 2011; 22:1879–1903.
3. McCarthy JR, Weissleder R. Multifunctional magnetic nanoparticles for targeted imaging and therapy. Adv Drug Delivery Rev. 2008; 60:1241–1251.
4. Jarzyna PA, Skajaa T, Gianella A, Cormode DP, Samber DD, Dickson SD, Chen W, Griffioen AW, Fayad ZA, Mulder WJM. Iron oxide core oil-in-water emulsions as a multifunctional nanoparticle platform for tumor targeting and imaging. Biomaterials. 2009; 30:6947–6954. [PubMed: 19783295]
5. Heesakkers RA, Futterer JJ, Hovel AM, van den Bosch HC, Scheenen TW, Hoogeveen YL, Barentsz JO. Prostate cancer evaluated with ferumoxtran-10-enhanced T2*-weighted MR imaging at 1.5 and 3.0 T: early experience. Radiology. 2006; 239:481–487. [PubMed: 16641354]
6. Guthi JS, Yang S-G, Huang G, Li S, Khemtong C, Kessinger CW, Peyton M, Minna JD, Brown KC, Gao J. MRI-visible micellar nanomedicine for targeted drug delivery to lung cancer cells. Mol Pharm. 2010; 7:32–40. [PubMed: 19708690]
7. Heymer A, Haddad D, Weber M, Gbureck U, Jakob PM, Eulert J, Noth U. Iron oxide labelling of human mesenchymal stem cells in collagen hydrogels for articular cartilage repair. Biomaterials. 2008; 29:1473–1483. [PubMed: 18155133]
8. Kester M, Heakal Y, Fox T, et al. Calcium phosphate nanocomposite particles for in vitro imaging and encapsulated chemotherapeutic drug delivery to cancer cells. Nano Lett. 2008; 8:4116–4121. [PubMed: 19367878]
9. Pan D, Caruthers SD, Hu G, Senpan A, Scot MJ, Gaffney PG, Wickline SA, Lanza GM. Ligand-directed nanobialys as theranostic agent for drug delivery and manganese-based magnetic resonance imaging of vascular targets. J Am Chem Soc. 2008; 130:9186–9187. [PubMed: 18572935]
10. Shin J, Anisur RM, Ko MK, Im GH, Lee JH, Lee IS. Hollow manganese oxide naonpartcles as multifunctional agents for magnetic resonance imaging and drug delivery. Angew Chem Int Ed Engl. 2009; 48:321–324. [PubMed: 19040234]
11. Nasongkla N, Bey E, Ren J, Ai H, Khemtong C, Guthi Jagadeesh S, Chin S-F, Sherry AD, Boothman David A, Gao J. Multifunctional polymeric micelles as cancer-targeted, MRI-ultrasensitive drug delivery systems. Nano Lett. 2006; 6:2427–2430. [PubMed: 17090068]
12. Hilger I, Andra W, Hergt R, Hiergeist R, Shubert H, Kaiser WA. Electromagnetic heating of breast tumors in interventional radiology: in vitro and in vivo studies in human cadavers and mice. Radiology. 2001; 218:570–575. [PubMed: 11161180]

13. Hilger I, Fruhauf K, Andra W, Heirgeist R, Hergt R, Kaiser WA. Heating potential of iron oxides for therapeutic purposes in interventional radiology. Acad Radiol. 2002; 9:198–202. [PubMed: 11918373]
14. Comes Franchini M, Baldi G, Bonacchi D, et al. Bovine serum albumin-based magnetic nanocarrier for MRI diagnosis and hyperthermic therapy: a potential theranostic approach against cancer. Small. 2010; 6:366–370. [PubMed: 20020469]
15. Weinstein JS, Varallyay CG, Dosa E, Gahramanov S, Hamilton B, Rooney WD, Muldoon LL, Neuwelt EA. Superparamagnetic iron oxide nanoparticles: diagnostic magnetic resonance imaging and potential therapeutic appliations in neurooncology and central nervous system in flammatory pathologies, a review. J Cereb Blood Flow Metab. 2010; 30:15–35. [PubMed: 19756021]
16. Corot C, Robert P, Idee JM, Port M. Recent advances in iron oxide nanocrystal technology for medical imaging. Adv Drug Delivery Rev. 2006; 58:1471–1504.
17. Lee ES, Shuter B, Chan J, Chong MS, Ding J, Teoh S, Beuf O, Briguet A, Tam KC, Choolani M. The use of microgel iron oxide nanoparticles in studies of magnetic resonance relaxation and endothelial progenitor cell labelling. Biomaterials. 2010; 31:3296–3306. [PubMed: 20116846]
18. Morales MA, Jain TK, Labhasetwar V, Leslie-Pelecky DL. Magnetic studies of iron oxide nanoparticles coated with oleic acid and Pluronic(R) block copolymer. J Appl Phys. 2005; 97:1–3.
19. Lim YT, Noh Y, Han JH, Cai Q, Yoon K, Chung BH. Biocompatible polymer-nanoparticle-based bimodal imaging contrast agents for the labeling and tracking of dendritic cells. Small. 2008; 4:1640–1645. [PubMed: 18819168]
20. Gupta AK, Wells S. Surface-modified superparamagnetic nanoparticles for drug delivery: preparation, characterization, and cytotoxicity studies. IEEE Trans Nanobiosci. 2004; 3:66–73.
21. Nkansah MK, Thakral D, Shapiro EM. Magnetic poly(lactide-*co*-glycolide) and cellulose particles for MRI-based cell tracking. Magn Reson Med. 2011; 65:1776–1785. [PubMed: 21404328]
22. Cruz LJ, Tacken PJ, Bonetto F, Buscho SI, Croes HJ, Wijers M, de Vries IJ, Figdor CG. Multimodal imaging of nanovaccine carriers targeted to human dendritic cells. Mol Pharm. 2011; 8:520–531. [PubMed: 21381651]
23. Xu C, Nieves MD, Ankrum JA, et al. Tracking mesenchymal stem cells with iron oxide nanoparticle loaded poly(lactide-*co*-glycolide) microparticles. Nano Lett. 2012; 12:4131–4139. [PubMed: 22769232]
24. Park J, Mattessich T, Jay SM, Agawu A, Saltzman WM, Fahmy TM. Enhancement of surface ligand display on PLGA nanoparticles with amphiphilic ligand conjugates. J Controlled Release. 2011; 156:109–115.
25. Fahmy TM, Samstein RM, Harness CC, Saltzman WM. Surface modification of biodegradable polyesters with fatty acid conjugates for improved drug targeting. Biomaterials. 2005; 26:5727–5736. [PubMed: 15878378]
26. Tantra R, Jing S, Pichaimutho SK, Walker N, Noble J, Hackley VA. Dispersion stability of nanoparticlees in ecotoxicological investigations: the need for adequate measurement tools. J Nanopart Res. 2011; 13:3765–3780.
27. Pinna N, Grancharov S, Beato P, Bonville P, Antonietti M, Niederberger M. Magnetite nanocrystals: nonaqueous synthesis, characterization, and solubility. Chem Mater. 2005; 17:3044–3049.
28. Sun S, Zeng H. Size-controlled synthesis of magnetite nanoparticles. J Am Chem Soc. 2002; 124:8204–8205. [PubMed: 12105897]
29. Sun S, Zeng H, Robinson DB, Raoux S, Rice PM, Wang SX, Li G. Monodisperse MFe_2O_4 (M=Fe, Co, Mn) nanoparticles. J Am Chem Soc. 2004; 126:273–279. [PubMed: 14709092]
30. Wang Y, Ng YW, Chen Y, Shutter B, Yi J, Ding J, Wang SC, Feng SS. Formulation of superparamagnetic iron oxides by nanoparticles of biodegradable polymers for magnetic resonance imaging. Adv Funct Mater. 2008; 18:308–318.
31. Wang L, Neoh KG, Kang ET, Shuter B, Wang SC. Biodegradable magnetic–fluorescent magnetite/poly(dl-lactic acid-*co*-α,β-malic acid) composite nanoparticles for stem cell labeling. Biomaterials. 2010; 31:3502–3511. [PubMed: 20144844]
32. Aderem A, Underhill DM. Mechanisms of phagocytosis in macro-phages. Rev Immunol. 1999; 17:593–623.

33. Win KY, Feng SS. Effects of particle size and surface coating on cellular uptake of polymeric nanoparticles for oral delivery of anticancer drugs. Biomaterials. 2005; 26:2713–2722. [PubMed: 15585275]

34. LaConte LEW, Nitin N, Zurkiya O, Caruntu D, O'Connor CJ, Hu X, Bao G. Coating thickness of magnetic iron oxide nanoparticles affects R_2 relaxivity. J Magn Reson Imaging. 2007; 26:1634–1641. [PubMed: 17968941]

35. Xie X, Zhang C. Controllable assembly of hydrophobic superparamagnetic iron oxide nanoparticle with mPEG-PLA copolymer and its effect on MR transverse relaxation rate. J Nanomater. 2011; 2011:1–7. [PubMed: 21808638]

36. Carroll MR, Huffstetler PP, Miles WC, Goff JD, Davis RM, Riffle JS, House MJ, Woodward RC, St Pierre TG. The effect of polymer coatings on proton transverse relaxivities of aqueous suspensions of magnetic nanoparticles. Nanotechnology. 2011; 22:325702–325709. [PubMed: 21772073]

37. Wang X, Yao C, Jiang Z. Conjugation of methotrexate to immunoglobulins kills macrophages by Fc receptor meidated uptake? Int Jnl Lab Hematol. 2008; 30:185–190.

38. Jordan MB, van Rooijen N, Izui S, Kappler J, Marrack P. Liposomal clodronate as a novel agent for treating autoimmune hemolytic anemia in a mouse model. Blood. 2003; 101:594–601. [PubMed: 12393630]

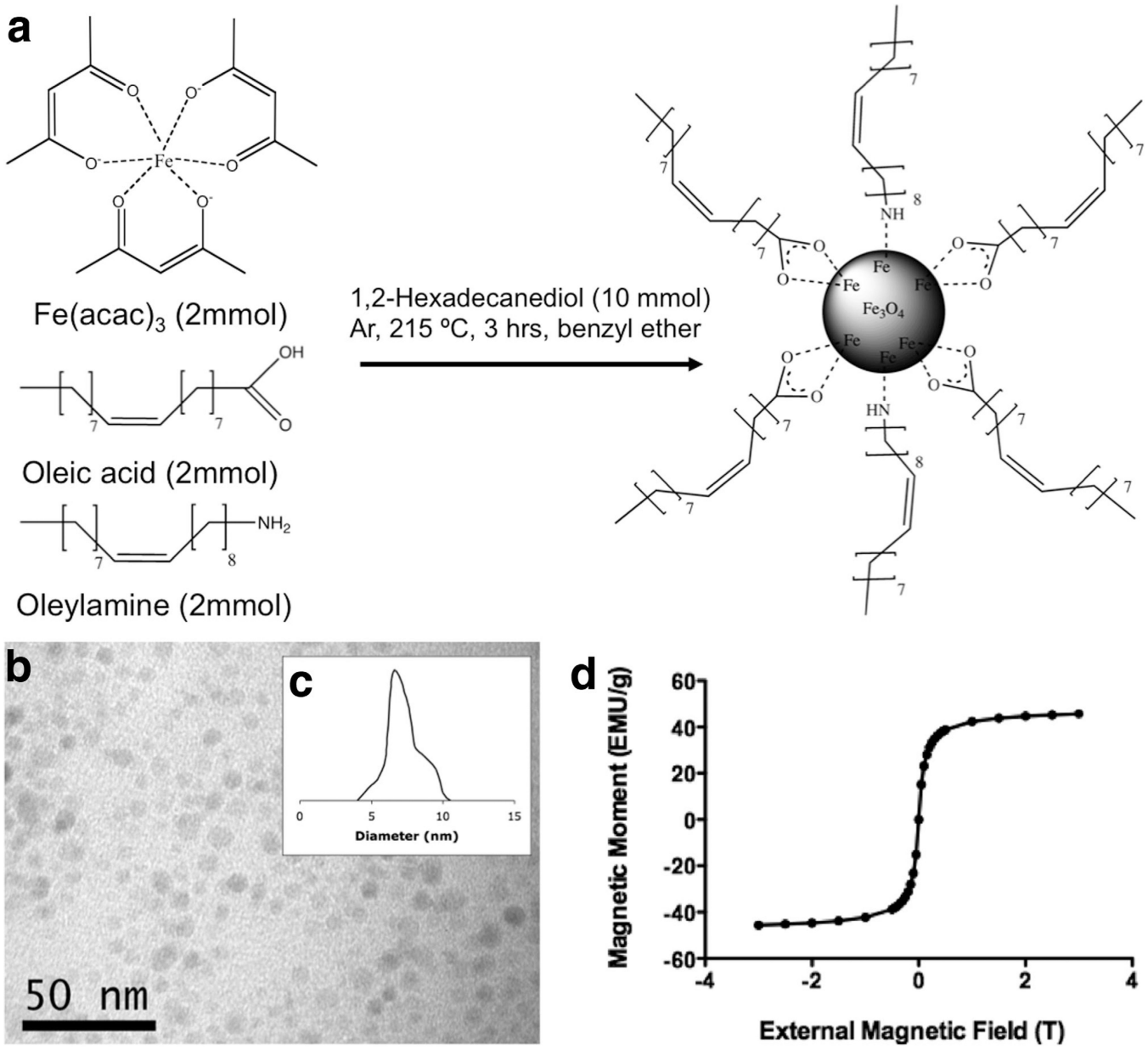

FIG. 1.

a: Synthesis of hydrophobic SPIO nanoparticles through high temperature reduction of $Fe(acac)_3$. **b**: TEM shows discreet nanoparticles with (**c**) average diameter being ~7 nm in diameter. **d**: SQUID shows SPIO nanoparticles with the absence of magnetic hysteresis.

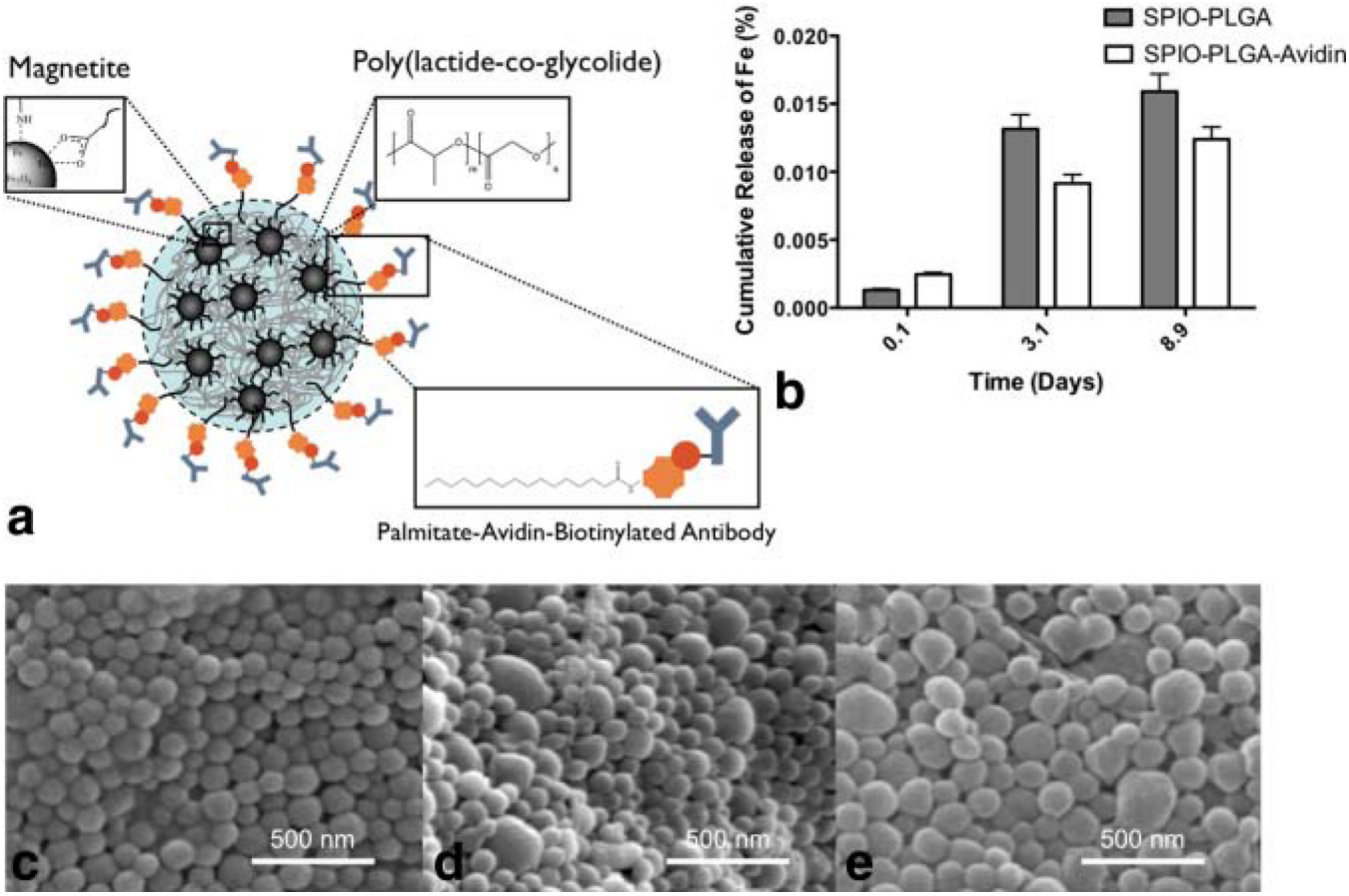

FIG. 2.

a: Schematic of SPIO-loaded PLGA nanoparticles with incorporated Avidin surface functionality for conjugating biotinylated antibodies. **b**: Inductively couple plasma mass spectrometer determination of negligible Fe release from PLGA nanoparticles in PBS at 37° C. Field-emission scanning electron microscopy of (**c**) blank PLGA nanoparticles, (**d**) SPIO-loaded PLGA nanoparticles, and (**e**) SPIO-loaded PLGA nanoparticles with Avidin surface functionality, respectively. [Color figure can be viewed in the online issue, which is available at wileyonlinelibrary.com.]

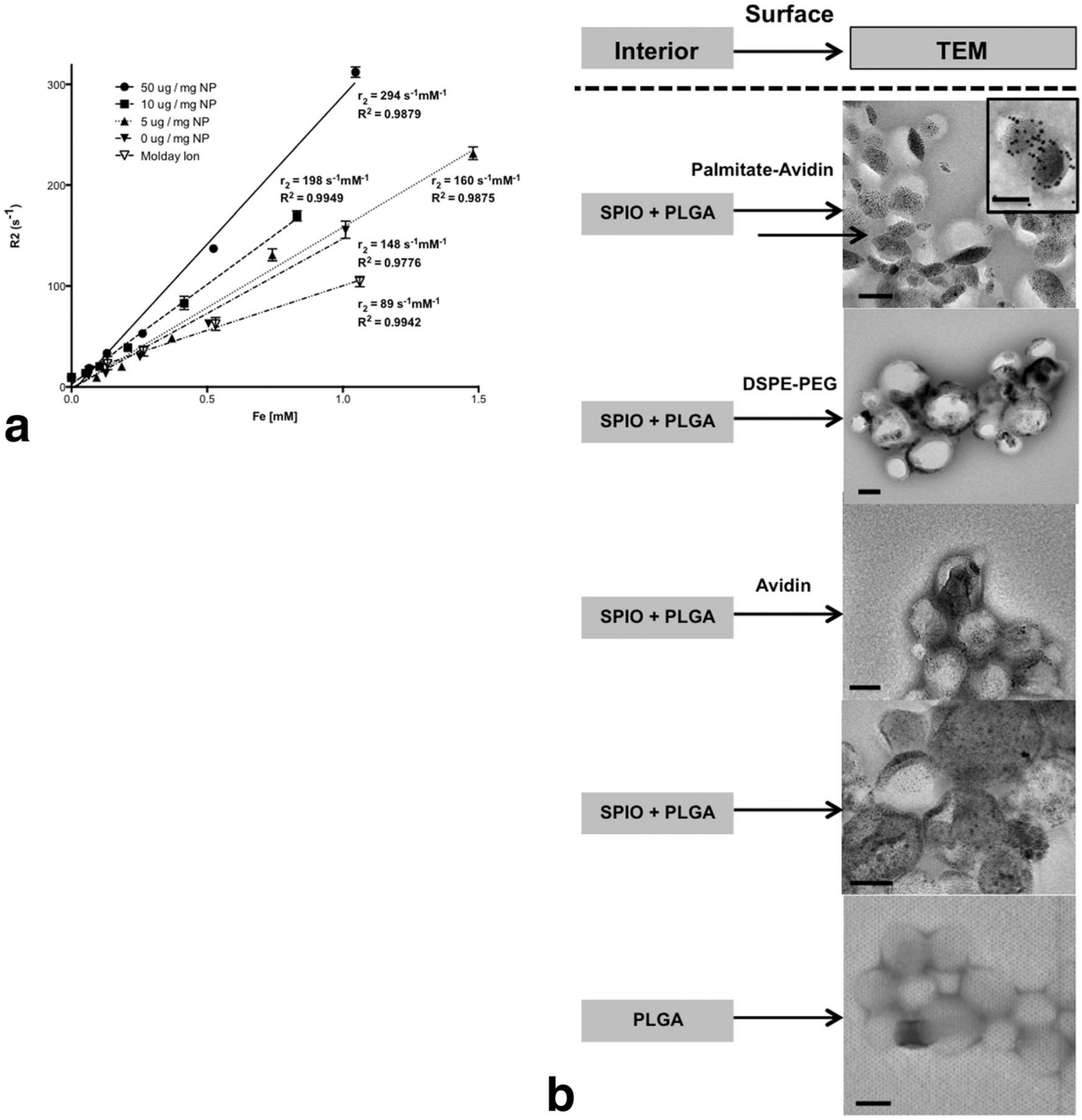

FIG. 3.

a: Spin-spin R_2 relaxation rate of SPIO-PLGA-Avidin with varying Avidin concentrations and SPIO-PLGA nanoparticles at different concentrations, compared with commercially available MR contrast agent, Molday Ion. **b**: TEM of various SPIO-PLGA nanoparticles including preparations with palmitate-avidin (with insert of nanoparticles decorated with biotinylated-gold), DSPE-PEG, soluble avidin, no surface modification, and blank PLGA nanoparticles as a control. All scale bars are 100 nm.

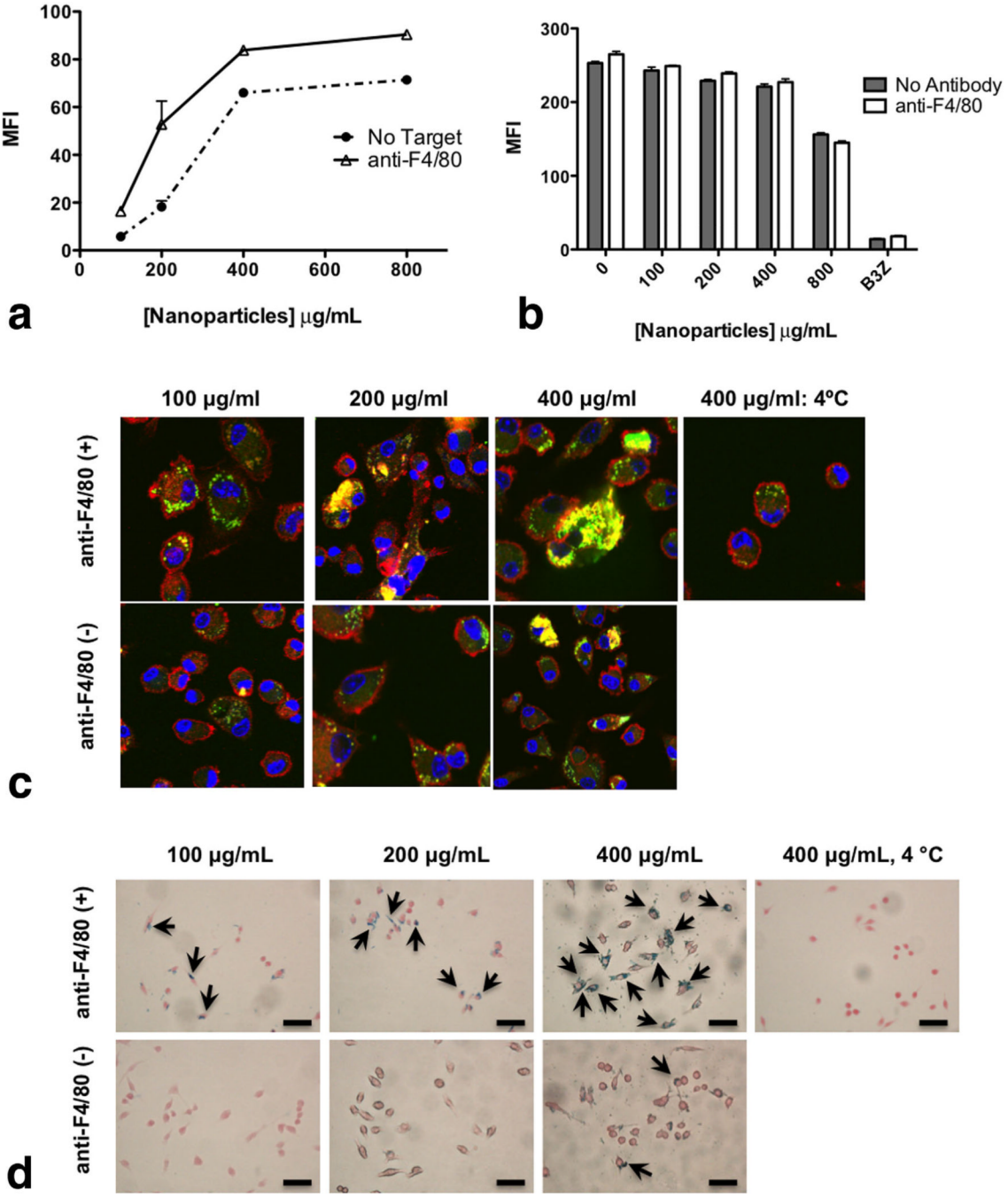

FIG. 4.

a: Nanoparticle internalization (both targeted and nontargeted) by macrophages using flow cytometry. BMDMs were exposed for 2 h to C-6-loaded nanoparticles (100–1000 μg/mL) with or without targeting with 5 μg/mL anti-F4/80 mAb per milligram nanoparticles. After 2 h, the cells were stained with CD11b-APC and fixed. Cells were gated on CD11b+ population and C-6 fluorescence intensity was measured for the gated CD11b+ population. **b**: Macrophages were assessed for metabolic activity by measuring the uptake of DiI-Ac-LDL in the cells: BMDMs were exposed to different concentrations of nanoparticles (100–800 μg/mL) for 2 h. After 2 h, cells were washed and Dil-Ac-LDL was added at a

concentration of 10 μg/mL in each well for 4 h at 37° C. After 4 h, cells were washed and analyzed for fluorescence at λ_{Ex}=520 nm and λ_{Em}=564 nm using flow cytometry. **c**: Internalization of targeted and nontargeted nanoparticles assessed by confocal microscopy. BMDMs were plated onto cover slips and exposed to C-6-loaded nanoparticles for 2 h. Cells were treated with or without targeting with anti-F4/80 mAb (5 μg/mg nanoparticles). After the indicated times, cells were fixed, permeabilized, and stained with Alexa Fluor® 548 phalloidin to label F-actin (red) and To-Pro-3 to label the nucleus (blue). Cells were visualized under a Zeiss confocal microscope using wavelengths 488, 568, and 633 nm. **d**: Internalization of targeted and nontargeted SPIO/C6-PLGA nanoparticles assessed by Prussian blue staining. Macrophages were plated onto cover slips and exposed to nanoparticles for 2 h. Cells were treated with or without targeting with anti-F4/80 mAb (5 μg/mg nanoparticles). Cells were then fixed with neutral buffered formalin, washed with PBS, then stained with ferrocyanide/hydrochloric acid mixture, and counterstained with Nuclear Fast Red. Images were obtained with a Nikon (TE2000-U) electron microscope. Scale bars are 100 μm.

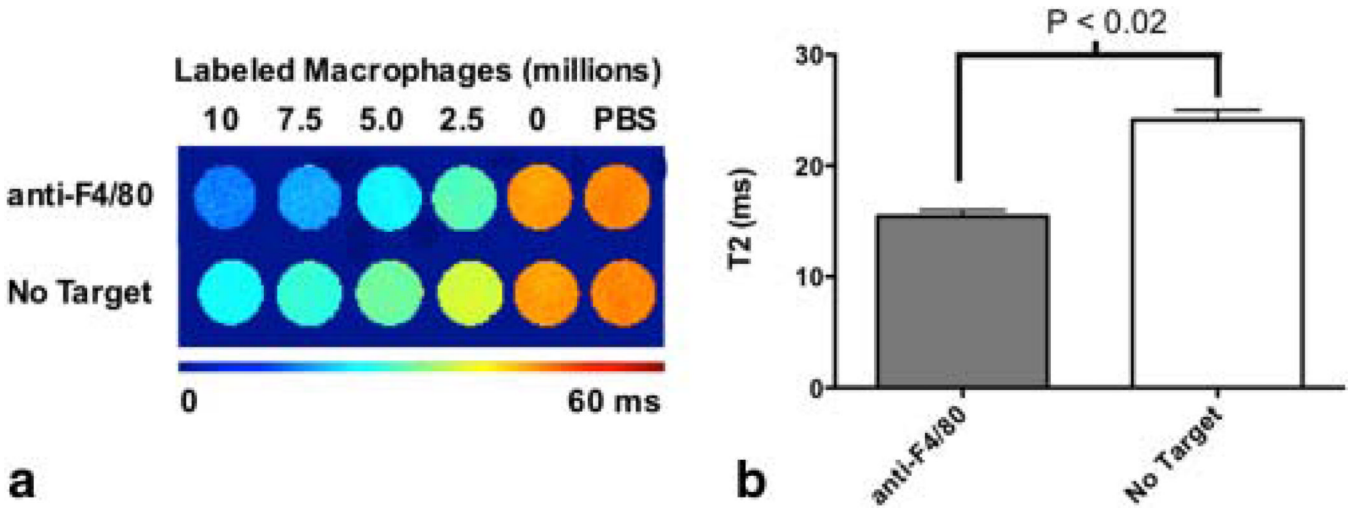

FIG. 5.

a: Representative T_2 maps of in vitro samples prepared with labeled macrophages incubated with different concentrations of SPIO-loaded PLGA nanoparticles (10×10^6, 7.5×10^6, 5×10^6, 2.5×10^6, and 0 labeled cells) with either no targeting or anti-F4/80. **b**: Cells with F4/80 showed a significant decrease in T_2 value compared with untargeted cells ($P<0.02$). [Color figure can be viewed in the online issue, which is available at wileyonlinelibrary.com.]

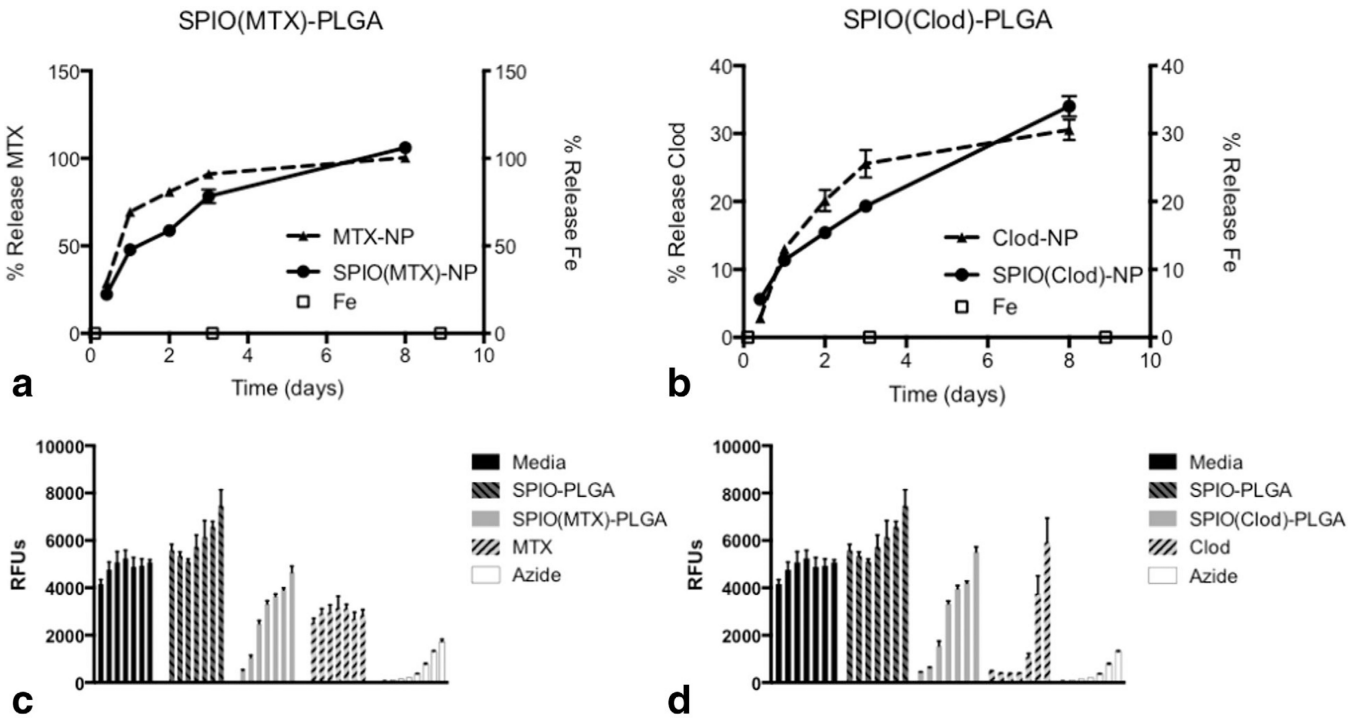

FIG. 6.

a: Controlled release of MTX from PLGA nanoparticles with and without SPIO loading shows 50% and 75% release, respectively, within 24 h with ~100% release after 8 days with negligible release of Fe. **b**: Controlled release of Clod from PLGA nanoparticles with and without SPIO loading shows 11% release within 24 h with ~30–35% release after 8 days with negligible release of Fe. Cytotoxicity was assessed using Cell titer blue: Macrophages were plated at a concentration of 50_4 cells per well in 96-well plates and were exposed to nanoparticles (starting with 8 mg/mL) containing both SPIO and either (**c**) MTX or (**d**) Clod at different nanoparticle concentrations and incubated for 24 h and compared with cells, magnetite-PLGA nanoparticles, soluble encapsulant (initial concentrations of MTX and Clod were 100 μM and 100 mM, respectively), and an azide control (initial concentration was 10 wt %). Cell titer blue (40 μL) was added to each well and incubated at 37°C for 3 h. Fluorescence was measured at λ_{Ex}=560 nm and λ_{Em}=590 nm.

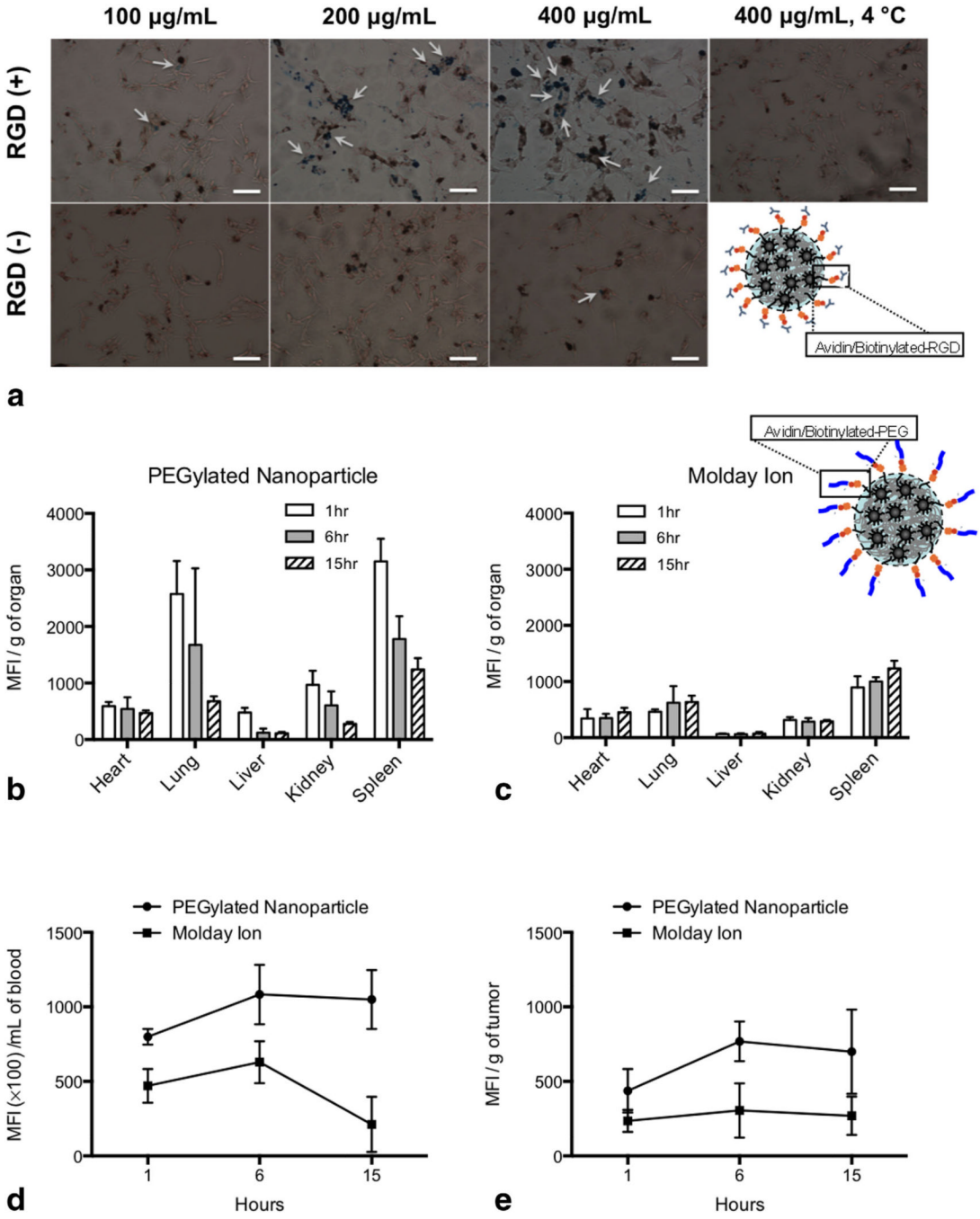

FIG. 7.

a: Internalization of targeted and nontargeted SPIO/C6-PLGA nanoparticles assessed by Prussian blue staining. B16 tumor cells were plated onto cover slips and exposed to nanoparticles for 2 h. Cells were treated with or without targeting with RGD peptide (5 µg/mg nanoparticles). Cells were then fixed with neutral buffered formalin, washed with PBS, then stained with ferrocyanide/hydrochloric acid mixture, and counterstained with Nuclear Fast Red. Images were obtained with a Nikon (TE2000-U) electron microscope. Scale bars are 100 µm. **b**: Biodistribution of SPIO/C6-PLGA nanoparticles decorated with avidin/biotin-PEG conjugates (b) and Molday Ion (**c**) in the heart, lung, liver, kidneys, and spleen at

1, 6, and 15 h. There were notable differences in biodistribution between the nanoparticles and Molday Ion in both the blood (**d**) and tumor (**e**).

Table 1

Commercial Superparamagnetic Iron Oxide Agents (15)

Commercial agent	Relaxivity (s^{-1} mM^{-1})[a]
Feridex/Endorem	120
Resovist	189
Combidex/Sinerem	65

[a] Relaxometric properties (mM^{-1} s^{-1}) at 1.5 T, 37° C.

Table 2

Nanoparticle Characterization

Nanoparticle	Size (nm)	Target wt % SPIO	Actual wt %	Relaxivity (s^{-1} mM^{-1})[a]
Blank PLGA	160±44	0	0	–
SPIO PLGA	250±69	19	13	160
SPIO PLGA Avidin	290±58	21	15	294

[a]Relaxometric properties (mM^{-1} s^{-1}) at 9.4 T, 37° C.

Table 3

Drug Loading

Drug	SPIO PLGA[a]
μg MTX/mg NP	1.4
μg Clod/mg NP	44.8

[a] Uncoated nanoparticles.